

Variogram Identification Aided by a Structural Framework for Improved Geometric Modeling of Faulted Reservoirs: Jeffara Basin, Southeastern Tunisia

Hayet Chihi,^{1,3} Mourad Bedir,¹ and Habib Belayouni²

Received 5 October 2011; accepted 8 February 2013
Published online: 10 March 2013

This article describes a proposed work-sequence to generate accurate reservoir-architecture models, describing the geometry of bounding surfaces (i.e., fault locations and extents), of a structurally complex geologic setting in the Jeffara Basin (South East Tunisia) by means of geostatistical modeling. This uses the variogram as the main tool to measure the spatial variability of the studied geologic medium before making any estimation or simulation. However, it is not always easy to fit complex experimental variograms to theoretical models. Thus, our primary purpose was to establish a relationship between the geology and the components of the variograms to fit a mathematically consistent and geologically interpretable variogram model for improved predictions of surface geometries. We used a three-step approach based on available well data and seismic information. First, we determined the structural framework: a seismo-tectonic data analysis was carried out, and we showed that the study area is cut mainly by NW–SE-trending normal faults, which were classified according to geometric criteria (strike, throw magnitude, dip, and dip direction). We showed that these normal faults are at the origin of a large-scale trend structure (surfaces tilted toward the north-east). At a smaller scale, the normal faults create a distinct compartmentalization of the reservoirs. Then, a model of the reservoir system architecture was built by geostatistical methods. An efficient methodology was developed, to estimate the bounding faulted surfaces of the reservoir units. Emphasis was placed on (i) elaborating a methodology for variogram interpretation and modeling, whereby the importance of each variogram component is assessed in terms of probably geologic factor controlling the behavior of each structure; (ii) integrating the relevant fault characteristics, which were deduced from the previous fault classification analysis, as constraints in the kriging estimation of bounding surfaces to best reflect the geologic structure of the study area. Finally, the estimated bounding surfaces together with seismic data and variogram interpretations were used to obtain further insights into the tectonic evolution of the study area that has induced the current reservoirs configuration.

KEY WORDS: Geophysics, reservoir, fault classification, compartment, stationary/nonstationary geostatistics, architectural model, tectonic evolution.

¹Georesources Laboratory, Centre for Water Researches and Technologies, University of Cartage, Borj Cedria Ecopark, P.O. Box 273, Soliman, Tunisia.

²Department of Geology, Faculty of Sciences of Tunis, University of Tunis El Manar, 1068, Tunis, Tunisia.

³To whom correspondence should be addressed; e-mail: hayet_chihi@yahoo.fr

INTRODUCTION

Geocellular modeling of reservoir architecture is a valuable tool in reservoir characterization, mainly in cases involving structurally complex reservoirs or subtle stratigraphy. Geostatistical methods are widely used in exploration and reservoir

modeling; they have the advantage of being able to quantify the spatial variability of geologic structures through a critical input, “the variogram.” Its estimation is a crucial stage in spatial prediction for improved 3D geometric model building and for management decisions.

The assumptions underlying the variogram’s definition, its modeling, and the principles of the linear model of regionalization have been detailed in many textbooks (e.g., Journel 1977; Edward and Srivastava 1989; Chilès and Delfiner 2012). Our primary objective in this study is to make a specific attempt to establish a robust relationship between the geology and the major features of variograms. This allowed us to develop a detailed and consistent geologic interpretation of variograms and, thus, to calibrate a mathematically consistent variogram model for a better, more rigorous, estimation of reservoir envelopes. This is particularly necessary in complex geologic settings, due to the intense tectonics affecting reservoirs. So far, only a few studies have dealt with this issue (e.g., Sahin et al. 1998; Chihi et al. 2007; Samal et al. 2011).

In the Jeffara (situated in southeastern Tunisia) case study presented here (Fig. 1), the reservoirs exhibit (i) at a large scale, a trend as they are within a generally down-tilted domain; and (ii) at a smaller scale, a division into compartments. However, careful consideration is required when using a stationary or a nonstationary geostatistical assumption in such a case (Chilès and Delfiner 2012; Chihi 2000; Chihi et al. 2000). On the other hand, seismic data were important (i) in view of the absence of outcrop analogs in the study area, and (ii) in providing extensive lateral coverage. In fact, in this study, they were used in the following analyses: (a) For defining the structural framework of the study area and for revealing subtle fault characteristics, such as type, continuity, direction, throw magnitude, dip, and dip direction, which resulted in their classification. This fault analysis is highly significant in describing the regional and local scale, geologic structures of the studied reservoirs and in establishing the fault hierarchy that has to be integrated in the modeling procedures. (b) For defining consistent variograms, describing their behaviors, and identifying their components over different length scales and in different directions. (c) For establishing appropriate relationships between each variogram component and the defined geologic structures: down tilting and compartmentalization.

Four important issues were addressed in this study. The first is to bring up new considerations on

the structural framework of the Jeffara Basin and, hence, a better knowledge of the potential subsurface reservoirs and a better understanding of their general architecture and areal extent. The second is to establish a methodology of variogram interpretation and modeling where the variance is decomposed into a number of components. The behavior of each variogram component is studied in light of geologic knowledge, and explained over different length scales in different directions. Therefore, one can identify the specific variogram structure which can be potentially used as a model for estimation procedure. The third is to estimate the faulted bounding surfaces of Lower Cretaceous reservoirs to illustrate not only the importance of a reliable variogram model but also the “fault parameter” integration in building geometric models that describe as well as possible the geologic reality. The fourth is to perform a synthetic analysis of the obtained results to study the tectonic evolution of the study area and its impact on the development of major structural elements: a general down tilting toward the Mediterranean Sea and a compartmentalization into numerous uplifted and downlifted structures along the NW–SE and NE–SW directions.

GEOLOGIC SETTING

The study area is part of the “Jeffara coastal plain” situated in southeastern Tunisia (Fig. 1). It is a northwest-trending collapsed block arranged parallel to the Jeffara escarpment, “Dhahar.” It is offset by a series of NW–SE-trending normal faults. The “Medenine Fault” (Castany 1954) constitutes a major structure dividing the area into two domains: a NE subsiding domain, and a SW high domain. The major potential reservoir systems considered in this study are situated in the NE subsiding domain, which is located approximately between latitudes 37°10′ and 33°45′N and between longitudes 9°00′ and 9°35′E, bounded to the north and east by the Mediterranean Sea, to the northwest by the Zarat–Gabes area, and to the southwest by outcrops. The subsiding Jeffara Basin is filled with thick sedimentary sequences consisting of Mesozoic to Neogene sediments (Rouatbi 1967). The Neogene sequence is thick and covers the study area. The majority of outcrops exposed in the study area is in the west side and consists mainly of the “Tebaga,” “Matmata,” and “Tejra” mountains. The structural framework and the fault patterns control lateral facies and

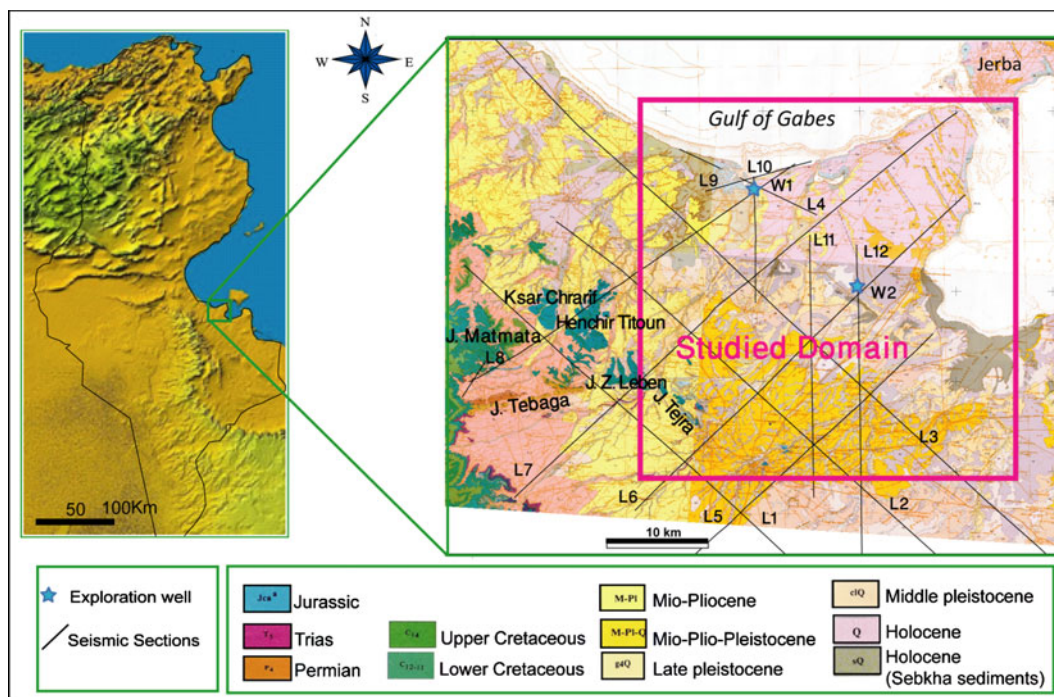


Figure 1. Geologic map and the distribution of seismic lines and well data in the study area.

thickness variations of the different sedimentary sequences.

In addition to thickness and facies variations, we noted the presence of several local and regional unconformities between Early Jurassic and Miocene formations, which we interpreted from 2D seismic data and exploration wells (Figs. 2–4, 16). Three major unconformities were identified and dated as Early Jurassic, Late Cretaceous, and Oligocene–Miocene. The Late Aptian–Early Albian and the intra-Aleg unconformities are considered to be minor events and are less well expressed compared with the others. These unconformities have been related to tectonic activity and reactivation of deep-seated faults in the Jeffara Basin (Castany 1954; Busson 1967; Bishop 1975).

Since the beginning of the Paleozoic, the Jeffara Basin has been affected by epeirogenic movements. Its tectonic history is generally believed to have been influenced by the Hercynian and Alpine orogenies (Busson 1967; Bishop 1975; Letouzey and Trémolières 1980; Burollet 1991; Klett 2001). A prolonged period from Late Permian to Senonian is dominated by extensional tectonics. Some short transpressive events correlated to the “Austrian phase” in Europe have been reported by various authors (Mzoughi et al. 1992; Bouaziz et al. 1998,

2002; Patriat et al. 2003; Bodina et al. 2010). These events intervened in the Middle Norian and in the Late Aptian–Early Albian. Extensional events were oriented along approximately N–S and NE–SW trending axes, whereas the Alpine compression was oriented along NW–SE. Many of the faults bounding the depositional sub-basins may have been inherited from the reactivated basement faults associated with the Devonian to Carboniferous (Hercynian) orogeny. Consequently, the present-day structural setting of the Jeffara domain is characterized by an array of structural features (folds, horst and graben) bounded by a complex fault system.

Most importantly, petroleum and water reservoirs are contained in carbonate rocks and sandstone sequences throughout the Jurassic, Cretaceous, and Tertiary series (Fig. 2): the Jurassic Techout and M’rabtine Formations; the Cretaceous Merbah Lasfer, Orbata, Fom El Argoub, Zebbag and Abiod Formations; and the Miocene Ain Ghrab Formation. These reservoirs are bounded and compartmentalized by the complex fault system, inherited from the succession of tectonic events. This study focuses on the Lower Cretaceous reservoirs. Owing to the vertical seismic resolution, seismic markers are not available for all these reservoirs (Scott et al. 1997). Thus, two mappable seismic sequences or “composite

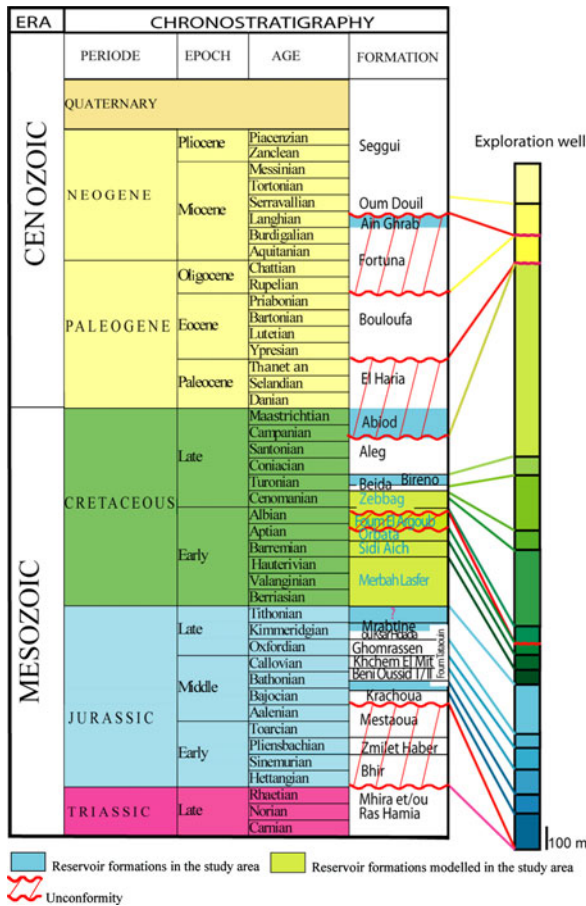


Figure 2. Stratigraphic column of Mesozoic Cenozoic units showing the main unconformities and reservoir occurrence in the study area.

reservoirs” were identified, each one containing many individual reservoir formations.

The first composite reservoir (Fig. 2) includes the Merbah Lasfer, Sidi Aich and Orbata Formations. Its upper boundary is the Aptian–Albian unconformity surface and its lower boundary is the Upper Jurassic surface. The sediments are composed of clastic alluvial materials from the Saharan Platform (Buroillet et al. 1978). The Merbah Lasfer Formation (Berrasian to Hauterivian) is mainly composed of sandstones and dolostones. Barremian rocks consist of Sidi Aich sandstones. Aptian rocks are mainly composed of limestones and dolostones of the Orbata Formation. (Bishop 1975; Salaj 1978; Entreprise Tunisienne d’Activités Pétrolières 1997).

The second composite reservoir includes the Albian to Cenomanian Zebbaga Formation (Fig. 2). It was deposited sealing unconformably the Orbata

Formation and is composed primarily of carbonate rocks. It is bounded by the Aptian–Albian unconformity surface on the bottom and the Upper Cenomanian on the top.

GEOLOGIC AND SEISMIC DATA EXPLORATION

The key objective of the current section is to determine the structural framework and, thus, to build fault network within the study area. Fault network building is a particularly crucial step in the modeling process, because faults compartmentalize reservoirs and play a key role in subsurface flow, whether faults are sealing barriers or drains. After collection and extraction of structural geologic data, they are used to generate a 3D architectural model of Lower Cretaceous reservoirs.

Data and Methodology

The available data come from a 2D seismic survey with 12 lines totaling about 200 linear kilometers and from two exploration wells (Fig. 1). Sonic, density, neutron porosity logs with lithostratigraphy (Fig. 2) are available from these two exploration wells. The seismic data were collected at an approximate average spacing of 10 km: four lines are oriented along NW–SE, five lines are generally oriented NE–SW, and three lines are oriented N–S (Fig. 1).

Seismic data acquisition, registration, and processing had been carried out in 1982 by the “Compagnie Générale de Géophysique (CGG)” in the so-called Kirchaou Petroleum Permit. The seismic line data had been acquired by split spread vibrator track source emissions of 20 s sweep and 10–60 Hz frequencies. The minimum line offset is 125 m, whereas the maximum line offset is 2,350 m. The distance between the source vibrator and point’s emissions is 50 m, and the geophone intertrace distance is 50 m. The number of traces per line is 96. The registration format is SEG B. The time reflection wave registration is 20 s, and the sampling rate is 4 ms. The filter frequencies used for registration is from 10 to 62.5 Hz, and the geophone frequency is 10 Hz.

Seismic reflector amplitude registration and presentation is in minimum phase. The seismic lines processing had taken into account all the treatment

stages from the static and dynamic corrections to the amplitude gain, the scan velocity, and deconvolution operations as well as the stack and migration processing. All the grid lines had been migrated, and the overall *data quality* is relatively good and adequate for our objective, which is to describe large-scale geologic structures of the studied domain. The quality of the data set worsens noticeably below the Top Jurassic horizon, making the selected times for the Triassic horizon somewhat uncertain. Moreover, due to data quality deterioration toward the SW of the study area, no seismic horizon could be identified along the seismic cross sections near the Medenine Fault zone.

As mentioned above, this study focuses on two mappable seismic sequences or “composite reservoirs” from the Lower Cretaceous, because of the vertical seismic resolution. Thus, the defined markers (Top Jurassic, Top Aptian, and Top Cenomanian) were detected on all 12 lines. Because these data are the property of “Entreprise Tunisienne d’Activités Pétrolières,” unfortunately, we are unable to show the precise positions of the seismic lines or to completely reproduce the seismic reflection data. Consequently, a single seismic profile (L6) (Fig. 3) was chosen to illustrate the reservoir compartmentalization; a second interpreted seismic line was converted and is shown as a line drawing in Figure 16.

Faults and seismic reflectors identification and interpretations were made (Fig. 3) manually, using two-way travel time (TWT) data sets with lithostratigraphy derived from the drilled exploration wells (Figs. 1, 2). Faults were mapped on each profile and, where possible, correlated between profiles (Fig. 5). Seismic horizons were identified with the local stratigraphy using data from exploration wells (Fig. 4) then, were correlated throughout the seismic grid (Fig. 3).

To insure accurate matching of horizons across the faults, the interpretations were confirmed in three ways: (i) fault classification: define the most important criteria to establish fault populations and hierarchy; (ii) horizon interpretations (Figs. 3, 4): take into account the fault classification to match strong reflectors across faults and determine reliable fault slip displacement; and iii) fault network building: use the interpreted seismic cross sections and the geologic maps to correlate fault traces and build the fault network throughout the study area (Figs. 3, 5).

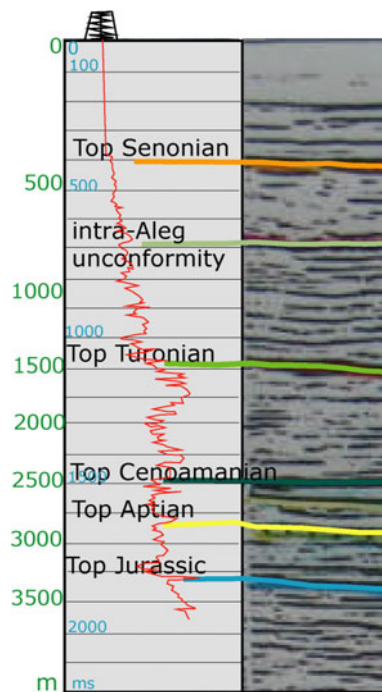


Figure 4. Seismic horizon identification and correlation with the local stratigraphy.

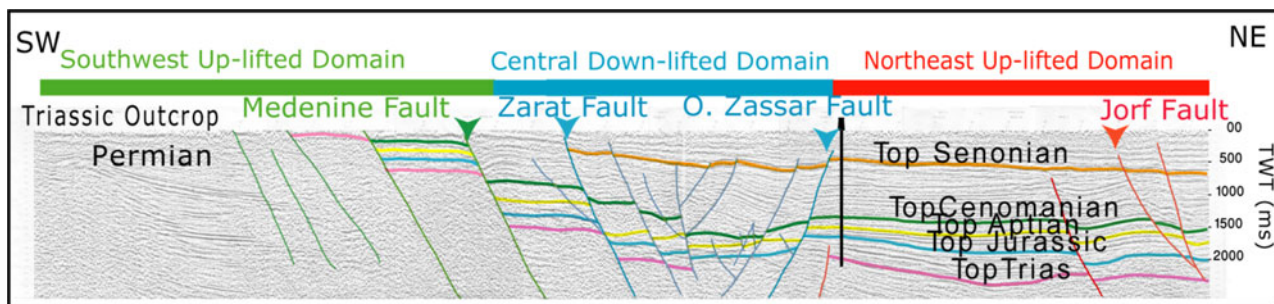


Figure 3. Interpreted seismic section L6 (see Fig. 1 for location) illustrating the normal faults and regional compartmentalization in the study area.

Fault Classification

To make a comprehensive analysis of the fault system in the Jeffara Basin, we defined some criteria for distinguishing fault populations. These criteria, according to Gauthier and Lake (1993) and Fossen (1996), can be generally classified into (a) genetic criteria that include timing or sequence of faulting (different tectonic events), type of faulting (reverse, strike-slip or normal) and relations to the deformation mode (pre-rift, syn-rift, gravity-driven or compaction-related, or tectonic); and (b) geometric criteria, which are based on differences in strike, dip, or dip-direction. Based on these criteria and on previous outcrop studies of the structural configuration of neighboring domains in the study area, within the Jeffara Basin (Busson 1967; Bouaziz 1990), all the mapped faults formed more or less at the same time. That is, they started to develop during the Hercynian phase.

The seismic data used here confirm (as it will be explained in the following sections) that the mapped faults in the study area show evidence of activities during different periods throughout the Mesozoic and Cenozoic. They affected the sedimentary sequences. Taking this into account, we deduce changes in fault activities throughout geologic time based on relative movements and amounts of displacement along affected sedimentary sequences. Therefore, our fault classification was mainly based on (i) type of faulting (i.e., reverse or normal), and on (ii) geometric criteria (i.e., strike, throw magnitude, dip, and dip direction).

For fault classification, we attempted to identify the main structures (seismic reflectors versus faults), and then we applied a coherence analysis (e.g., cross correlation or semblance) to seismic data to recognize prominent geologic structures that characterize the study area at local and regional scales. Three tasks were carried out. In the first task, we identified the main discontinuities like faults or seismic horizons marking unconformities on each seismic section. In the second task, we identified the considered horizons on the right and the left side of the fault. In the third task, we identified structural subdomains or compartments. In each task, we applied a coherence analysis (local and regional resemblance) based on a priori knowledge (i.e., fault behavior and geologic history) as explained below.

Local Resemblance

We identified the geometric criteria of each fault: fault type, fault direction, throw magnitude,

dip, and dip direction. Then, we compared the similarity of sequences of reflectors on both sides of a fault, to identify horizons that do or do not have counterparts on either sides of each fault. Finally, we classified the mapped faults according to their previously defined characteristic (type, direction, throw magnitude, dip, and dip direction) and to the sequence of reflectors on both sides of every fault.

Regional Resemblance Recognition

This task involves the combination of interpreted sequences of horizons and “mapped faults” in terms of geologically local and regional valid match for the whole study area to define geologically consistent compartments that are bounded by faults. The different compartments identified are compared, at large scale, between two or more successive parallel seismic sections. This analysis was very useful to understand the reservoirs’ architecture and their extension in the study area, and it has several important implications for geologic modeling procedures, which allowed us to achieve the following. Build the fault network within the study area. Define a geographic subdivision of the study area into “regular sub-areas” or compartments where the variability of depth is relatively “homogeneous” from a geostatistical point of view. Depth values in a compartment are expected to have strong similarities. Establish the fault hierarchy that has to be integrated in the modeling procedures.

Fault Network Building

Fault correlation analysis consists of “manually building” the fault network using four main sources of information that were previously geo-referenced in a unique geographic system: (i) seismic sections interpretations, providing structural parameters including attitude of bedding, thrusts, normal fault; (ii) geological maps of the area showing and describing locations of outcrops and their limits, tectonic elements, and seismic lines (Fig. 1); (iii) topographic data represented by contour lines; and (iv) lithostratigraphic correlations and geologic cross sections reconstructed by analyzing borehole data (Chihi et al. 2012).

The manual method of building fault network was carried out in four steps. (i) Faults were

identified and mapped “manually” on each seismic section (Fig. 3). (ii) For a given fault, we located the intersection (called a trace) of a seismic horizon and a fault line. (iii) Then, this trace is projected on the seismic survey shot-point grid to define its spatial position (X and Y coordinates). (iv) Finally, fault traces are correlated on the grid of the seismic sections that were previously superposed to the geologic map, by linking traces from cross section to cross section. Outcrop data were also efficiently used to predict fault spatial localization and extension by correlation of seismic fault traces with outcrop limit, in the west side of the study area [seismic lines L1, L7, and L8 (Figs. 1, 5)]. Fault correlations were confirmed by fieldwork and by lithostratigraphic correlation based on borehole data covering the Jeffara de Medenine aquifers (Chihi et al. 2012).

For geologic validity, crossover tests of (i) previously interpreted seismic horizons; (ii) mapped faults; and (iii) induced correlated faults, throughout the seismic grid superposed to geologic map were repeatedly carried out until a fault network honoring the known geologic history of study area, is obtained. Note that the correlation procedure was restricted to fault whose occurrences (based on the fault classification criteria) are easy to define objectively on a number of parallel profiles.

The Resulting Structural Framework

The structural interpretations using the seismic data showed that the most prominent faults identified and correlated in the study area display NW–SE strikes with throws toward either the NE or SW. These faults, from SW to NE (Figs. 3, 5), are the Tejra-Medenine fault, the Medenine fault, the Zarat fault, the Lella Gamoudia fault, the Oum Zassar fault, and the Jorf fault. Several minor, unevenly spaced faults were mapped using the seismic cross sections of the study area, but these minor faults are not correlated because they are rarely continuous and could not be correlated between the seismic profiles. All of the mapped major and minor faults allowed us to compartmentalize the study area and to build a system of uplifted and downlifted structures within a generally down-tilted domain. Therefore, the Jeffara Basin can be subdivided into three different compartments as shown in a seismic section striking SW–NE, in the direction of subsidence (i. e., toward the NE), and showing an overall strong reflectivity (Fig. 3; Table 1).

The SW uplifted domain pertains to the western part of the study area, where sediments are deformed by NW–SE oriented normal faults, dipping about 70° to the NE. These normal faults have large throws of up to 1,000 m (Figs. 3, 5). These structures, which are considered as first-order faults, are from NW to SE (Table 1): the Tejra-Medenine fault has large throw of about 800 m and generates topographic scarps of Triassic sediments; and the Medenine fault is the most significant fault with the largest throw of about 1,000 m. Late Cretaceous to Quaternary sediments are uplifted. Thus, the reflector sequence is composed of Top Triassic to Top Cenomanian horizons, in which the Top Senonian horizon is uplifted and is no longer recognized to be on the left side compartment of the Jeffara fault (Fig. 3).

The central downlifted domain is affected by variably oriented smaller faults. Within this domain, Upper Jurassic to Quaternary sediments are downlifted, the reflector sequence is composed of Top Triassic to Top Senonian (Table 1).

The major fault marking the SW border of the central domain is the Zarat fault. It is a NW–SE oriented normal fault, dipping about 70° to the NE. It has large throw of about 400 m. The Oum Zassar fault delimits the NE border of the graben. It is a NW–SE oriented normal fault; it shows variable dips ranging between 50° and 70° to the SW and variable slip displacements. The Zarat and Oum Zassar faults are considered second-order faults.

Faulting occurs throughout the study area, but is most concentrated in this domain between the Zarat and Oum Zassar faults. In this sector, minor faults have small throws. These minor faults were generally not taken into account in the estimation procedure, because they are rarely continuous and could not be correlated between the seismic profiles.

The NE uplifted domain of the study area is the most stable domain. It is deformed by NW–SE oriented normal faults, dipping about 70° to the NE. The Jorf fault is the main one. It has a small throw and affects moderately the sediments. It is considered a third-order fault (Table 1). Upper Jurassic to Quaternary sediments are uplifted, and the reflector sequence is composed of Top Triassic to Top Senonian (Table 1).

We emphasized that, based on the structural framework defined above and from the point of view of modeling, the Medenine fault is the major trend that played a key role in the compartmentalization of the study area, allowing for the definition of a NE subsiding domain and a SW weakly subsiding, high domain. The major potential reservoir systems

considered in this study are situated in the NE subsiding domain.

GEOMETRIC MODELING

A consistent 3D reservoir architectural model was constructed in several steps on the basis of the

available data sets and using the Geostatistical software ISATIS (Geovariances 2012). In this section, we present the modeling steps and results for the two Lower Cretaceous “composite reservoirs” by mapping the boundaries of each one. The mapping is based on measurements of topographic elevation Z (measured in seconds) of the “composite reservoirs”

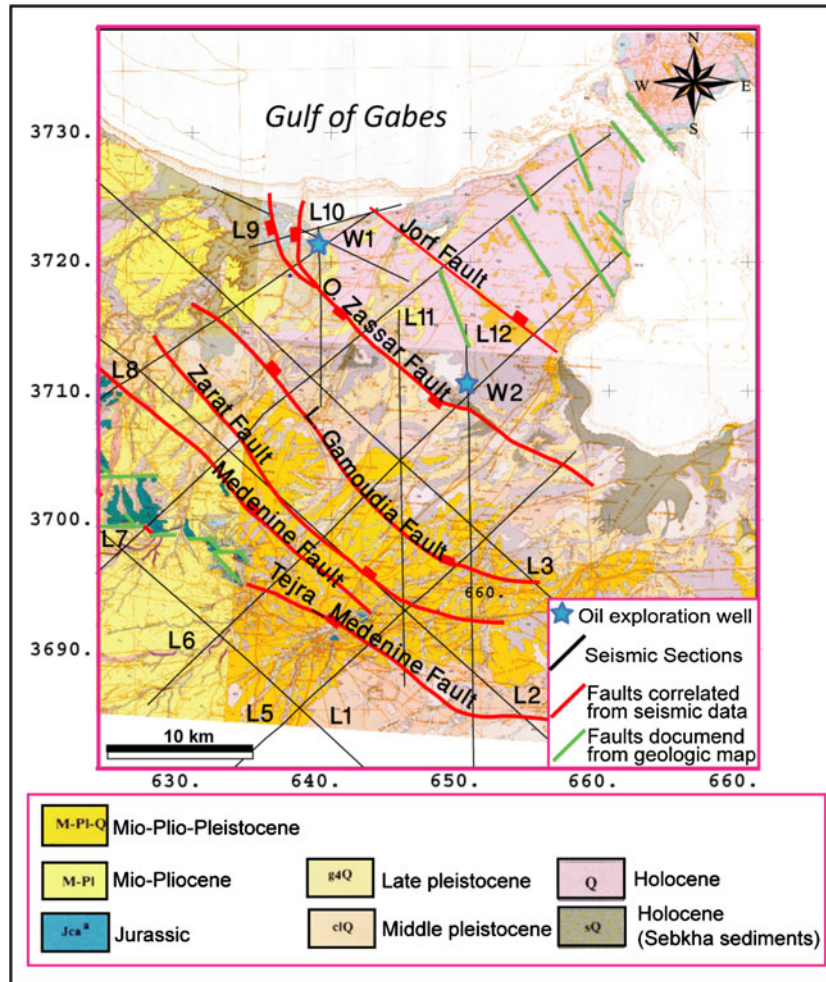


Figure 5. Map of fault network interpreted through correlation between seismic profiles in the NE Jeffara Basin.

Table 1. Hierarchy of Faults and Definitions of Compartments in the Study Area

Fault Population	1st Order Faults	2nd Order Faults	3rd Order Faults
Throw (m)	800–1,000	up to 400	<100
Compartment	SW uplifted domain	central downlifted domain	NE uplifted domain
Name(s) of fault(s)	Medenine, Tejra-Medenine	Zarat, Lella Gamoudia Oum Zassar	Jorf
Dip direction	NE	NE SW	NE
Recognized horizon within the compartment	Top Triassic to Top Cenomanian; the Top Senonian horizon is uplifted and is not recognized	Top Triassic to Top Senonian	Top Triassic to Top Senonian

boundaries on each seismic profile (Jurassic, Aptian, and Cenomanian horizons). The surface boundaries were then estimated by geostatistical methods. The workflow of the geostatistical modeling involves the following major steps: (i) data base conception; (ii) variographic analysis; (iii) surface estimation; and (iv) 3D geometrical model construction by a 3D visualization of the kriged bounding surfaces. The large number of normal faults, which are clearly visible on seismic sections, was integrated in the modeling approach, because they are important in the delineation of the reservoir configuration.

Data Management, Input Data

Twelve seismic cross sections, two exploration wells and four assembled geologic maps (Fig. 1) were used to provide direct information on subsurface geology needed for the spatial modeling of the different bounding surfaces. However, these raw data alone are useless without careful and methodical processing and interpretation that we summarize into two steps. First, data georeferencing is a crucial step in the modeling process, whereby all available layers of information are combined and organized in a common coordinate system. This must cover the entire study area and must be precise enough so as not to lose or distort information. Second, digitizing, of the seismic data that we provided in paper format and definition of, the limits of reservoir units (Jurassic, Aptian, and Cenomanian horizons) through geologic interpretation and manual seismic time selection. We scanned all the already interpreted seismic cross sections and then digitized elevations in the three identified horizons. We then recorded the depth variable (measured in seismic time in seconds) in an input 2D time-referenced data file (X , Y , depth variable of each selected seismic marker). The fault system that compartmentalizes the reservoir units was introduced as a 2D-referenced data file, attached to the database of the selected seismic markers, and taken into account in the interpolation and statistical procedures. Each fault is defined by different attributes, among which the “priority value.” It is an “importance level” assigned to a given fault to represent its throw magnitude and its impact on surface geometry. The “priority value” represents a key attribute in setting up a hierarchical distinction between faults, which is based on the fault classification established during the fault network building as presented above. Accordingly, the “Medenine

fault,” which is the main discontinuity in the area, was given the first priority value. The remaining faults, considered to be secondary discontinuities, were given lower priority values. The fault parameters were inferred during the different steps of geometric modeling.

Variographic Analysis

Variographic analysis (Chilès and Delfiner 2012) is one of the most important steps in a geostatistical study; it characterizes the spatial structure of the variable by means of consistent probabilistic models that are estimated through the variogram function. A variogram measures and describes the spatial variation of regionalized variables as a function of the distance (Olea 1994). The behavior of this variability function at short and long distances reveals several spatial characteristics of data. Depending on spatial characteristics of data, the variogram function is modeled with a mathematical function that will be used for estimation.

In our case study, the complex geologic setting described above (Fig. 3) and below (Figs. 9, 16, 17), induced by repetitive fault activities, resulted in complex variogram behavior for each faulted bounding surface. We fitted theoretical models to the experimental variograms taking into consideration geologic parameters that we have defined as constraints in the interpolation procedure. The methodology we followed to model the experimental variograms includes three main steps. (i) Experimental variogram calculation of the depth variable in each “composite reservoir” boundary: Jurassic, Aptian, and Cenomanian horizons (Figs. 2, 3); (ii) Variogram behavior interpretation: the variogram behavior must be interpreted and related to geologic and structural information that control the reservoirs configuration; and (iii) Variogram fitting: in light of geologic knowledge, a mathematically consistent model was adjusted and used for a better, more rigorous, estimation of the Lower Cretaceous reservoir envelopes.

Experimental Variogram Calculation

The calculation of experimental variograms involves a series of decisions, with respect to direction, lag increment and their respective tolerance, depending on prior data analysis and geologic

knowledge. In this study, the experimental, mean, and directional variograms were calculated for each depth variable (of Jurassic, Aptian, and Cenomanian horizons) for a maximum distance of 30,000 m, along the seismic profiles, to discern the possible nested structures at small and large scale (Figs. 6–8). Variograms were also calculated for four specified directions (E–W, NE–SW, N–S, and NW–SE) to determine the anisotropic behavior of the depth variable. It is considered anisotropic when its spatial variability changes with direction.

Variogram Behavior Interpretation

The interpretation of variogram behavior is needed to establish structural relationships between geologic variations and observed variogram components for reliable variogram modeling. The behavior of experimental variograms shows various components, called nested structures (Figs. 6–8). We recognized the following three main nested structures through the analysis of mean and directional variograms (Fig. 9). (i) The first nested structure is a locally stationary structure. The variogram curve shows that the variance increases and reaches a sill. (ii) The second nested structure is a drift or a non-stationary structure. The variogram curve shows that the variance increases continuously beyond the variance. (iii) The third nested structure is a hole effect.

The variogram curve shows that within the first local stationary structure, the variogram reaches a lower sill then it increases to reach a second one expressing a cyclicity phenomenon in the depth variability.

The directional variograms show an anisotropic behavior, as the scale of the three nested structures changes from one direction to another. Both sill and range change with direction for the stationary structure. The drift component changes also with direction. The variable depth presents a good example of zonal anisotropy variable that we describe as follows (Figs. 6–8). (i) The stationary structures are more strongly expressed in the E (D1) and NW (D4) directions. (ii) The drift is more strongly expressed in the NE direction (D2). (iii) The hole effect is more pronounced in the northern direction (D3). The behavior of each structure is shown to reflect a defined geologic feature. Our geologic knowledge provided valuable guidance in the interpretation of the variogram behavior (Fig. 9).

The Stationary Structure. The locally stationary structure is related to the depth variability, at a small scale, within each compartment (Fig. 9). The variograms show a sill lower than the sample variance for the Jurassic “Depth” (Fig. 6). For the Aptian “Depth” and the Cenomanian “Depth,” the variograms show sills that are higher than the sample variances (Figs. 7, 8). In general, the sill increases with decreasing depth of the surfaces (from Jurassic

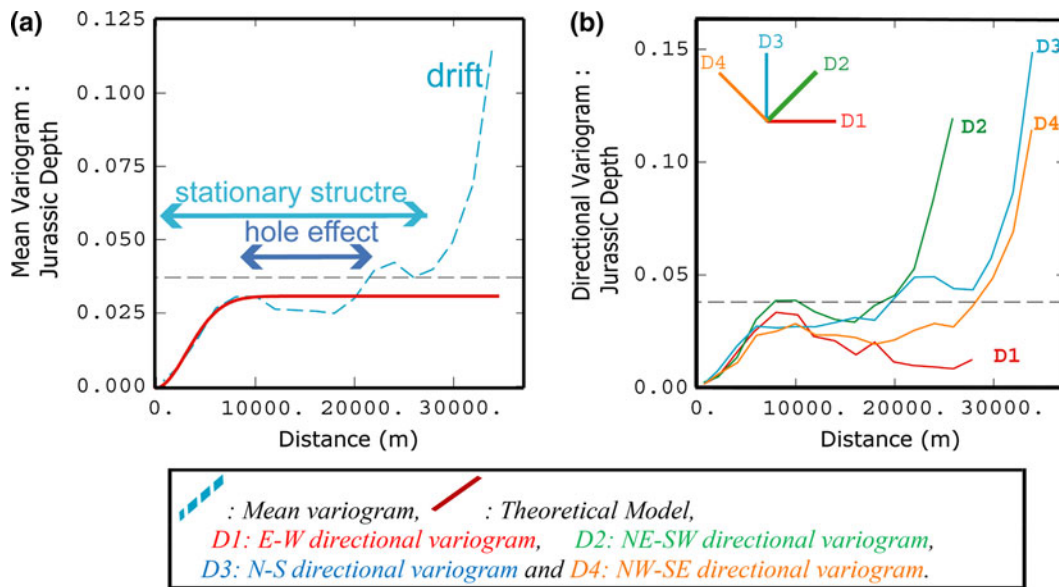


Figure 6. (a) Mean variogram of depth in the Jurassic horizon. (b) Directional variograms of depth in the Jurassic horizon.

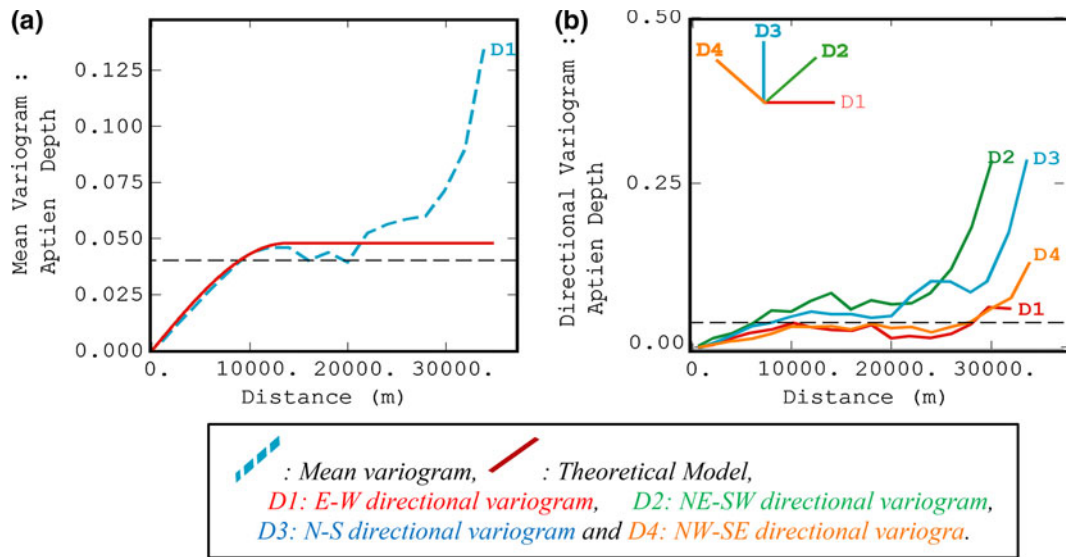


Figure 7. (a) Mean variogram of depth in the Aptian horizon. (b) Directional variograms of depth in the Aptian horizon.

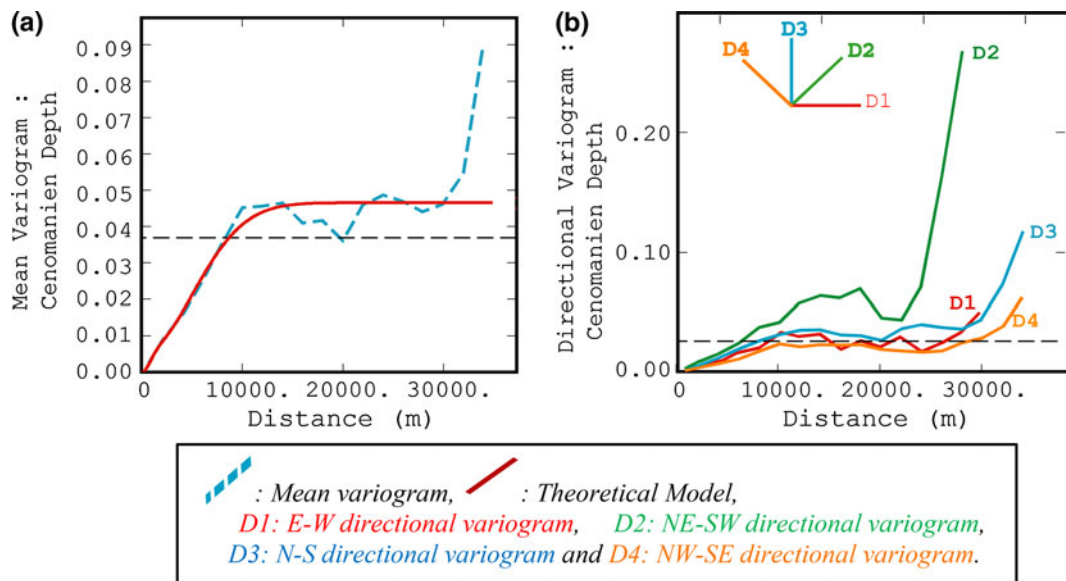


Figure 8. (a) Mean variogram of depth in the Cenomanian horizon. (b) Directional variograms of depth in the Cenomanian horizon.

to Cenomanian). The range increases with decreasing depth of the surfaces (from Jurassic to Cenomanian) (Figs. 6–8). The maximum spatial correlation was found to be 7,900 m for the Jurassic surface. It was estimated to be about 13,000 m for the Aptian surface and 14,453 m for the Cenomanian surface.

The Drift. The drift structure reflects the continuous increase of depth at the large scale within the overall down-tilted study area. The anisotropic behavior shown by the directional variograms reproduces the variation of the down tilting rate, which is highest in the NE direction (D2). The drift increases with

Table 2. Theoretical Models for Adjusting the Structural Variability of the Depth Variables

Variables	Model	Parameters
Jurassic depth	Gaussian	$\gamma(h) = 0.0031 \left[1 - \exp\left(-\left(\frac{h}{7,900}\right)^2\right) \right]$
Aptian depth	Spherical	$\gamma(h) = 0.0045 \left[\frac{3}{2} \frac{h}{12,980} - \frac{1}{2} \left(\frac{h}{12,980}\right)^3 \right]$
Cenomanian depth	Gaussian	$\gamma(h) = 0.005 \left[1 - \exp\left(-\left(\frac{h}{1,963}\right)^2\right) \right] + 0.0045 \left[1 - \exp\left(-\left(\frac{h}{12,980}\right)^2\right) \right]$

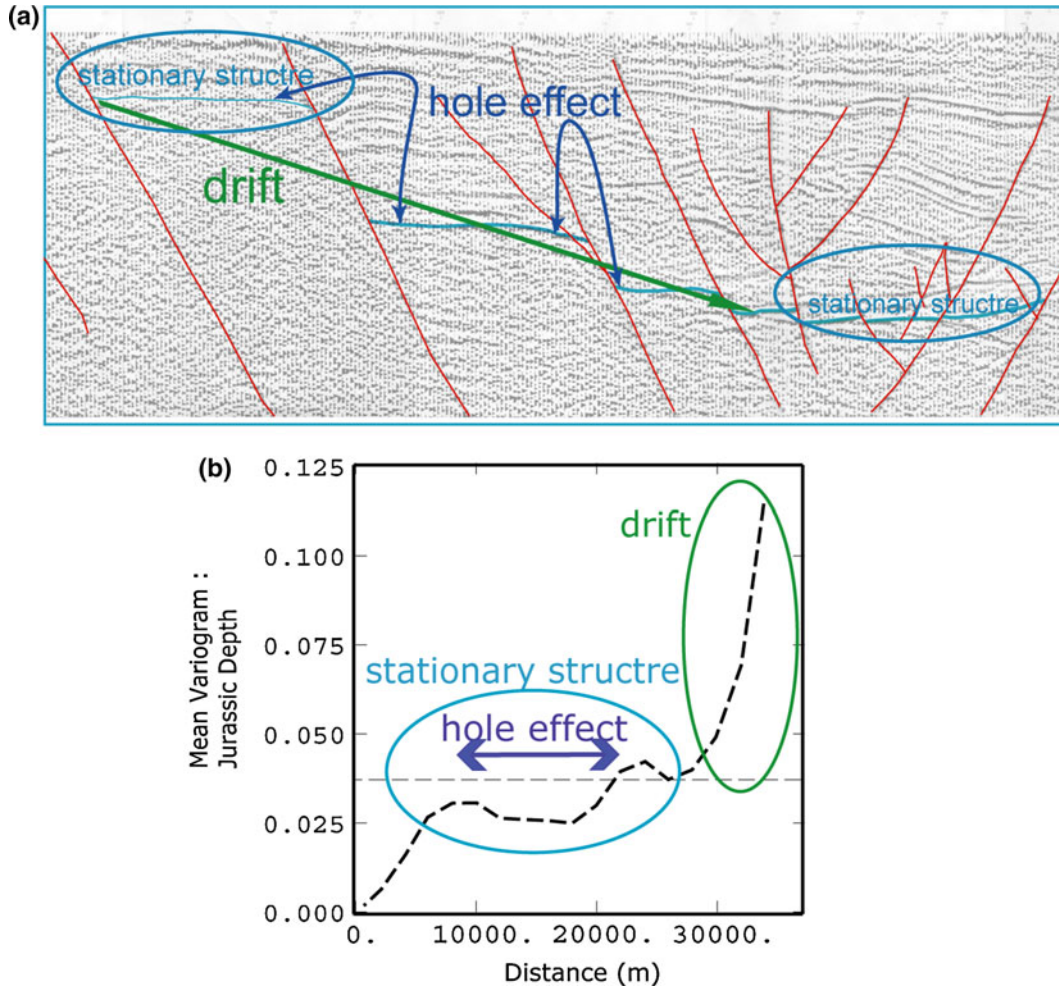


Figure 9. Geologic features (and hole effect) interpreted from a seismic section (a: exaggerated version of seismic line L6 in Fig. 3) and corresponding mean variogram components of the Jurassic horizon (b). The drift component illustrates the significant variation of the depth and thus the down tilting surface boundary, the stationary structure describes the limited variability of the depth within each compartment, and the hole effect expresses the cyclicity of the fault effect on the surface.

increasing depth of the surfaces (from Cenomanian to Jurassic). This may be explained by renewed pulses of tectonic activity mainly along the NW–SE extensional fault throughout geologic times. The

resulting amount of fault displacements along the affected areas may be intensified for older layers and more specifically from Cenomanian to Jurassic surfaces.

The Hole Effect. The hole effect reveals a spatially repetitive structure (Fig. 9). The faults cut the surfaces at many locations, the throw is increasing from one fault to another from the SW to the NE. Thus, the depth increases considerably from one compartment to an adjacent downlifted one. The hole effect is related to a repetitive jump in the depth variability from one compartment to an adjacent downlifted one. The hole effect is more clearly shown for the Jurassic surface. It is attenuated for the Aptian and Cenomanian. This is linked, as explained above (for the drift component of the variogram), to renewed pulses of tectonic activity mainly along the NW–SE extensional fault throughout geologic times.

Variogram Fitting

To measure spatial continuity, an experimental variogram has to be fitted with a theoretical model, as regards (i) Variogram components and parameters, (ii) previous geologic interpretations, so that it reflects our understanding of the reservoir geometry and continuity (Yarus and Kramer 2006; Gringarten and Deutsch 1999), and (iii) interpolation conditions.

The variographic and geologic analyses had shown that the variogram behavior is characterized by two major features: (i) at a small scale, a stationary structure related to the variability of depth within each compartment; and (ii) at a larger scale, a trend structure as the compartments belong to a generally down-tilted domain. Various models, each describing the variable correlation for a component of the total variance, can be combined as nested structures (Goovaerts 1997). However, it is very useful to assess the importance of each variogram component involving the geologic factor controlling the behavior of each structure and the interpolation conditions of the different surfaces. Therefore, we adopted the following three assumptions to select the theoretical functions for adjusting the experimental variograms: (i) The drift feature is imposed by the compartmentalization scheme; the depth increases from one compartment to another (Figs. 3, 9). (ii) The neighboring samples must be located within the considered compartment, between fault boundaries (Fig. 10). The model parameters must be inferred from variogram values at only a few distance classes. Accordingly, the variograms have to be fitted on the basis of their behavior toward small and medium distances, only the stationary behavior is taken into account for depth interpolation. (iii) Furthermore, taking into account the similarity of

the directional variograms at small and medium distances, the average experimental variogram was judged to be representative of the spatial structure of the data (Figs. 6–8). Based on these assumptions, we fitted the mean variograms with stationary (Gaussian and spherical) structures with ranges scaling from 7,900 to 14,000 m (Table 2). These distances were considered to be large enough to define an appropriate neighborhood for the estimation.

Modeling of Surfaces

The mapping of each bounding surface was based on (i) the spatial continuity analysis of the “depth variable” as detailed above and on (ii) kriging estimation. We performed kriging interpolation (Matheron 1982) by defining the estimation grid and the neighborhood parameters (Fig. 10) using the ISATIS geostatistical software (Geovariances 2012).

The Estimation Grid

The estimation grid (Fig. 10a) of the study area domain was defined so as to include all the surfaces and to minimize as far as possible the extrapolation at the corners of the grid. We then defined a 2D grid with the following parameters (Fig. 10a): origin at $X = 630,000$ m and at $Y = 3,690,000$ m; cell dimensions: $dx = dy = 500$ m; and number of cells: $n_x = 65$, $n_y = 82$. Consequently, the kriging had to be performed for 5,330 elementary estimation cells covering the entire study area.

Implementation of the Neighborhood Selection

The selection of the neighborhood was subject to a certain number of constraints to insure the continuity of the estimator and to achieve maximum precision (Fig. 10b). These constraints concerns first the *regional variability* and second the *local variability*.

Regional Variability. The study area was divided into compartments where the variability of the depth is assumed to be relatively “homogeneous.” For this, we employed a technique whereby geologic faults are integrated and considered as barriers. For each target point located inside a given

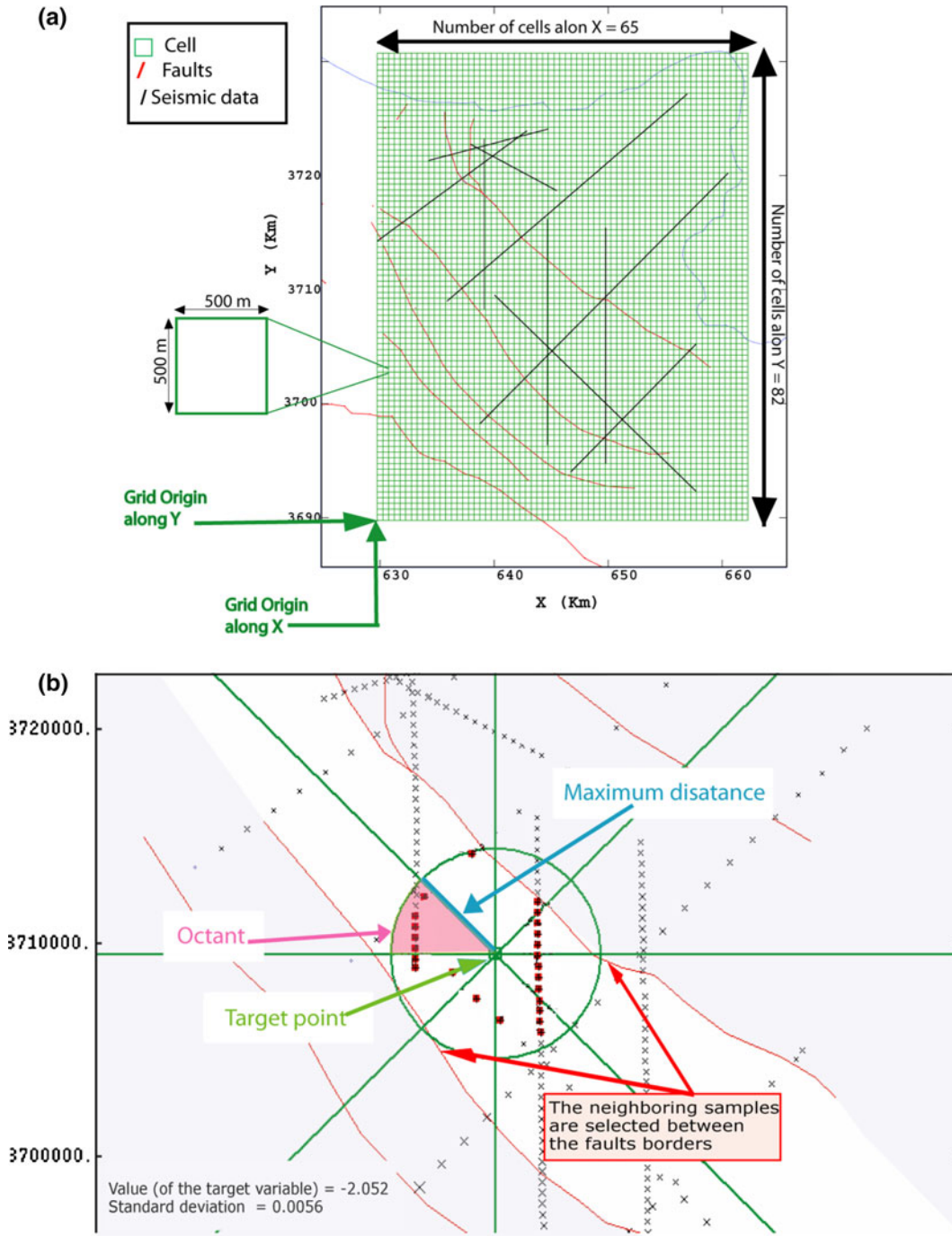


Figure 10. Grid discretization used for surfaces estimation (a) and parameters used for selecting neighboring samples (b). The test window shows the data set, faults, samples chosen for estimation, and the results of the kriging estimation. The neighboring points are distributed over eight angular sectors within the “neighborhood window” a circle of 8-km radius. The data points located in the shaded area cannot be taken for estimating any target point in the central compartment.

compartment, the search neighborhood procedure is performed so that the neighboring samples used for estimation are located only within the considered compartment, between fault boundaries. No sample located outside the faults bounding the considered compartment is ever selected for estimation.

Local Variability. For each local estimation inside the compartment of interest, we used only the immediate neighbors of a point to be predicted so as to respect the spatial continuity/variability of the phenomenon under study. To achieve this, we worked with a moving “local neighborhood” including a limited subset of data, the immediate neighborhood of a point to be estimated, to obtain a small data variance. Then, we used an “octant search” strategy, whereby the neighborhood is divided into eight octants centered on the node of the grid being estimated and the data points used as a neighborhood are selected so as to have the same neighborhood density in all of the octants. This allows to sample in every direction, as uniformly as possible and to insure interpolation continuity.

To deal with the *spatial distribution* of the data, which is characterized by a high density along the seismic lines and a low density across, the “maximum distance (dmax)” parameter is chosen large enough, without exceeding the range of the variogram, to allow the selection of the neighborhood among a sufficient number of seismic profiles to insure good coverage. The above process makes it possible to obtain a sufficiently continuous interpolator. The previously mentioned constraints led to the selection of the following parameters, moving neighborhood, maximum distance (dmax) of 7,000 m, eight angular sectors and five points taken as a neighborhood in each angular sector.

Standard Deviation Map

The estimation of uncertainty is very important because it gives the limits of probable values of depth at every point. The uncertainty is characterized through the kriging standard deviation and depends on the spatial distribution and configuration of the data points.

In general, the kriging standard deviation increases as the standard deviation of the data increases, and it decreases as data are closer to locations where estimations are made. However, the kriging standard deviation is essentially independent of the data values used in the estimation. The only link between the

kriging standard deviation and data values is through the variogram. Therefore, we adopted the following strategy to increase the surface accuracy by reducing the standard deviation: (i) For the surface estimation procedure, we applied a restricted kriging system that incorporates three restrictions: one for regional variability, the second for local variability, and the third for dealing with the spatial distribution of data points. These three restrictions are assured through the implementation of the “neighborhood selection” by integrating “fault parameter,” moving neighborhood, the octant strategy, and the maximum distance parameter previously discussed. (ii) Concerning the variogram, we opted for stationary structures to model the variograms, based on the variographic analysis to honor the data variance inside each compartment (see the “[Variographic analysis](#)” section above for more details).

We should emphasize the importance of the “picking error range” when digitizing seismic time horizons, because an excessive range in the picking error may give large uncertainties: first when calculating the variogram, the uncertainty will be expressed as nugget effect; and second when estimating the different surfaces, the uncertainty will be expressed as a kriging standard deviation.

The experimental variograms are quite continuous, and do not show a nugget effect at the origin (Figs. 6–8). This proves that the picking error is negligible and does not increase the surface estimation error. When the variogram structures are carefully chosen and the “neighborhood selection” is implemented on the basis of the above-mentioned three restrictions according to the data configuration and geologic assumptions, satisfactory results are obtained such as those presented on the kriging standard deviation map of the Jurassic depth (taken as an example) (Fig. 11).

Figure 11 shows that the surface estimation procedure gave satisfactory results. This is evident along the seismic profiles where the data density is the highest and where the kriging standard deviation is the lowest (i.e., <0.02 s), particularly at and around intersections of profiles, which are due to consistency of data values. In addition, inside the meshes formed by seismic profiles, the estimation is sufficiently precise because the values of the kriging standard deviation are in the range of 0.02–0.03 s. Moreover, it is only at the periphery of the investigated territory that the kriging standard deviation is greater than the standard deviation of the observed data, up to 0.19 s and that it is a consequence of a border effect. Furthermore, the quality of the

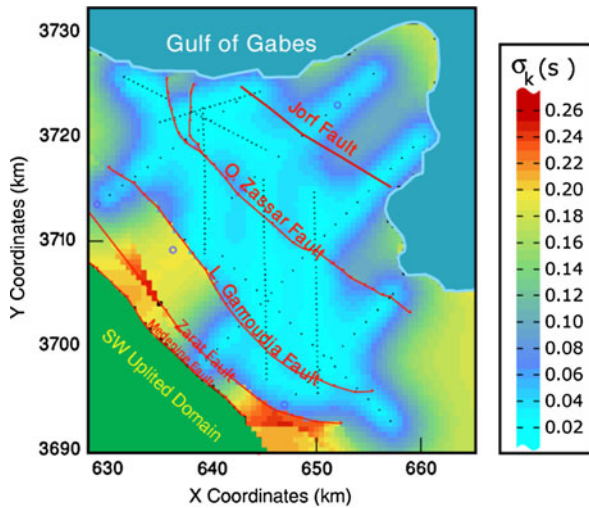


Figure 11. Kriging standard deviation map of the Jurassic horizon.

seismic data is often poor near the Medenine fault (as explained in the “[Data and methodology](#)” section), which makes the precise interpretation of horizons difficult. The precision is low in the SW compartment where the data are scarcer.

Consequently, the above interpretation of the reliability obtained by examining the data density and uncertainty estimation can be helpful in characterizing the likely role of geologic factors on the obtained depth maps. Hence, we base our interpretation of the tectonic features and, more generally, of the geology only in the reliable areas of the estimated maps of the Top Jurassic, Top Aptian and Top Cenomanian.

RESULTS AND DISCUSSION

Figures 12–14 show the final geometric reconstruction of the Top Jurassic, Top Aptian and Top Cenomanian isochrones maps by using the above defined parameters under a stationary assumption. Figure 15 displays the stacking of the two “composite reservoirs.” For better structural interpretations, we drew a suitable color-scale chart to define depth intervals within each surface; the depth intervals were compared with each other, from the oldest surface to the youngest one, to acquire surface geometry details. This allowed us to (i) apply a trend surface analysis to identify the main structural elements at regional and local scale within the study

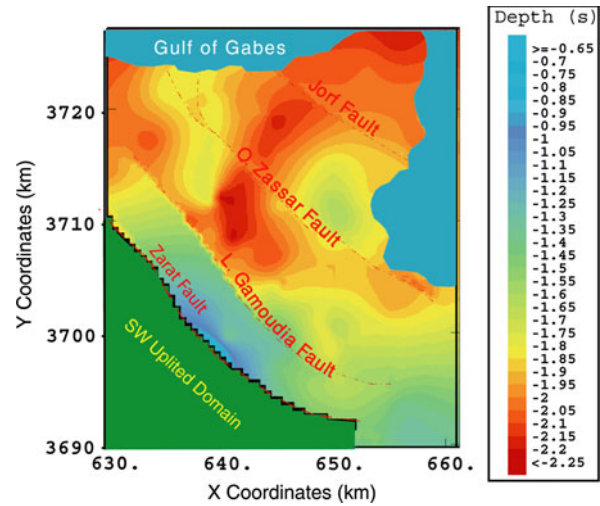


Figure 12. Top Jurassic isochrones map. At a regional-scale, the Jurassic surface shows generally increasing depths from land to the Gulf of Gabes, indicating that the whole area is generally tilted toward the north and the northeast directions. At a local scale, this down-tilted domain shows the individualization of several high and dropped structures initiated along the NW–SE and the NE–SW normal faults.

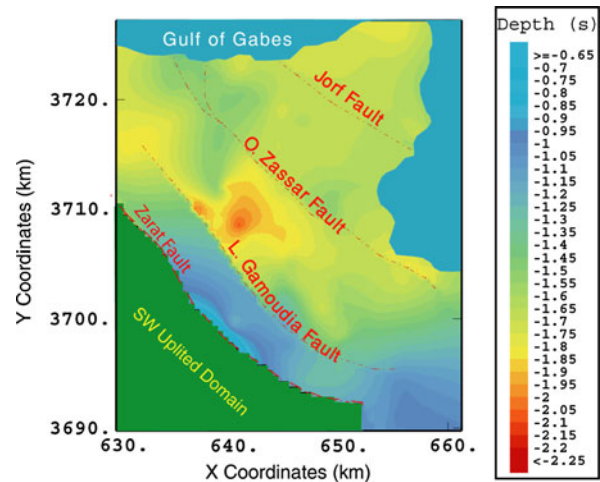


Figure 13. Top Aptian isochrones map. The Top Aptian depth map keeps, in general, the same geometric shape and the major structural elements, as the Top Jurassic depth map; however, these structures are not clearly expressed.

area, and (ii) to deduce the tectonic evolution that led to the current configuration of the studied reservoir. Both tasks were performed taking into account not only the modeled surface maps but also the original seismic data interpretation and the geologic assumptions deduced from the variographic analysis.

Structure Recognition on the Estimated Surfaces

Variations in color in Figures 12–14 depict depth variability of the estimated surfaces at local and regional scales. We carried out a trend surface analysis for the entire study area, or for specific zones, such as localities showing gentle or steep

slopes, for illustrating a uniform aspect or changes in slope intensity and/or in the gradient direction, to evaluate regional and local dips.

The time structure maps (Figs. 12–14) show the areal extent of several structural elements that were indicated by earlier interpretations on seismic lines. The maps clarify the continuity and spatial relationship of the structural elements. Conclusions are made first for the Jurassic surface (Fig. 12), and then generalized for the Aptian and Cenomanian surfaces (Figs. 13, 14).

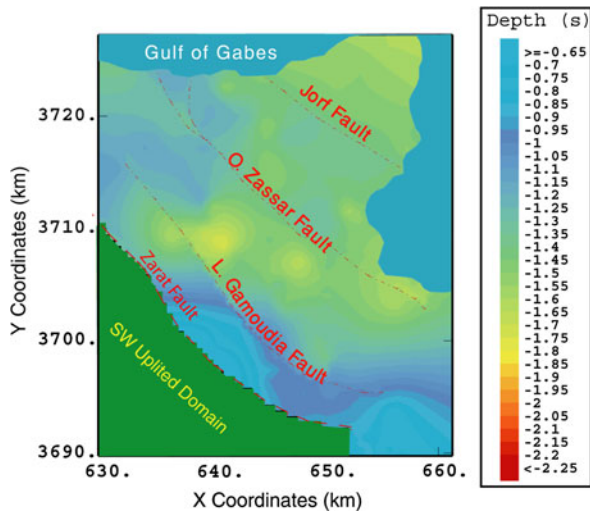


Figure 14. Top Cenomanian isochrones map. The Top Cenomanian depth map keeps, in general, the same geometric shape and the major structural elements; however, these structures are not clearly expressed as in the Top Jurassic and the Top Cenomanian depth maps.

The Depth Map of the Top Jurassic

The depth map of the Top Jurassic reservoir depicts the distribution of subsurface structures at regional and local scales (Fig. 12).

At a regional scale, the Jurassic surface shows generally increasing depths from land to the Gulf of Gabes. It presents irregular gradients parallel to the front of the NW–SE normal faults, indicating that the whole area is generally tilted toward the Mediterranean Sea (Fig. 12). Based on directional trend analysis carried out for the entire area, keeping in mind that the map presents steep gradients parallel to the front of the normal faults with an overall trend in the NW–SE direction, the faults are curvilinear and assumed to change their dip angle depending on their

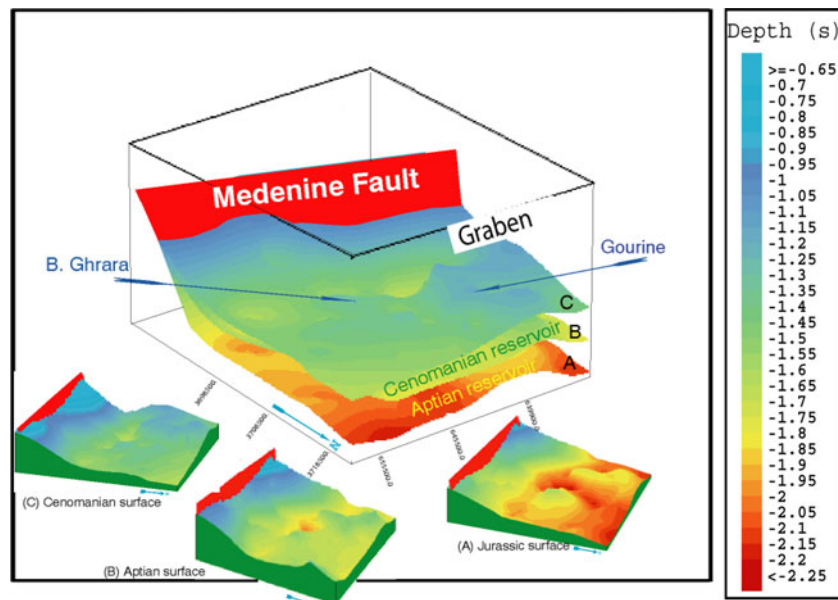


Figure 15. 3D geometric model of the lower cretaceous reservoirs from a NE perspective. 3D rendering of bounding surface geometries using faults interpreted from seismic data, from an approximately NE perspective.

local orientation. Faults are directed NW–SE in the northwest zone of the study area and dip to the northeast causing a NE down tilting of the Jurassic surface. In the south of the study area, they are directed E–W and dip toward the north causing tilting to the N. The Jurassic Top presents a third gradient in the NW direction, but it is gentler than the first two. In this context, the anisotropic behavior of the surface trend is revealed above through the variographic analysis (see “[Variogram behavior interpretation](#)” section above). Figure 6 reproduces the directional variation of the down tilting rate, which is higher in the NE direction. Furthermore, although the Top Jurassic within this generally down-tilted domain confirms the complex structuring of the Jeffara Basin, it nevertheless demonstrates the major role played by the NW–SE-trending normal faults in the area. Accordingly, within this down-tilted domain, horst and graben structures are clearly expressed as structures initiated along the fault systems (Figs. 3, 12, 17). The Jeffara Basin can be subdivided into three different compartments, as pointed out on the interpreted Jurassic map (Fig. 17) and on the profile cross section (Fig. 3): the Uplifted Domain in the southwestern sector of the study area, the Central Downlifted domain and the NE Uplifted Domain.

At a local scale, a detailed analysis of the trend surface is fitted to specific areas; we noted two facts (Fig. 12):

- (i) Slope intensity variation along the major NW–SE normal faults. This is clearly visible, for example, on the steepest slope and the gentler one (the gradient direction is generally to the NE) alongside the “Zarat fault” delimiting the SW border of the Central downlifted domain. It is a NW–SE-

oriented normal fault; it shows variable dips ranging between 50° and 70° to the NE and variable throw (Figs. 3, 12).

- (ii) Slope variation (in intensity and direction) transversely to major NW–SE normal faults. Steep slopes have preferred orientations, and are associated with elevated structures in the NW, SE and E–W directions. The depth map shows the individualization, within the Northern Jeffara domain, of several high zones depicted in the interpreted Jurassic map (Fig. 17). One of these is an anticline, located on the NW side of the study area (Gourine). It has a complex shape trending nearly N80E, it is wider toward the north and narrower toward the south. Small normal faults cut across the anticline flanks (Figs. 16, 17), dropping the western and the eastern limbs and moving them downward. The eastern fault dips steeply eastward and, therefore, gives an asymmetric shape to the anticline structure. The second high zone, a vertical uplift, is located in the central eastern side of the study area (Bou Ghrara) (Fig. 17). It could be interpreted as an uplifted structure generated by mainly NW–SE normal faults, the Zarat fault dipping about 70° to the SW and the Jorf fault NE dipping about 70° to the NE (Fig. 3). This structure is also affected by NE–SW trends as shown in Figure 16. These NE–SW trends create a distinct compartmentalization of the reservoirs along the NW–SE direction. Thus, the Jeffara Basin can be subdivided into three different compartments, as shown on the interpreted Jurassic map (Fig. 17): the Bou Ghrara

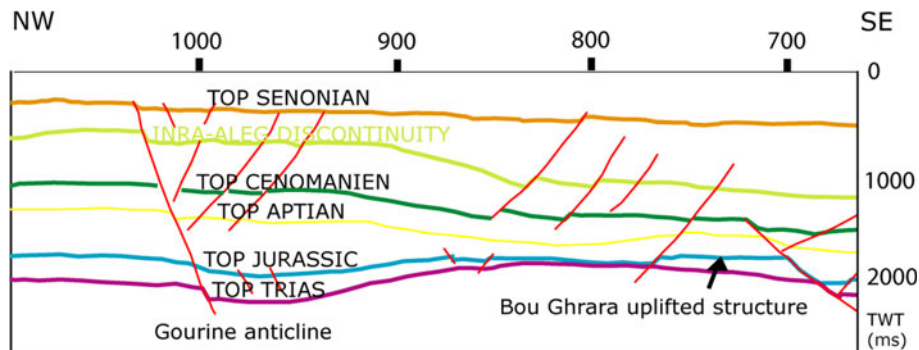


Figure 16. Interpreted regional seismic profile, showing the NE–SW normal faults, the preserved extensional geometry, and the structural inversion in the NE Jeffara Basin.

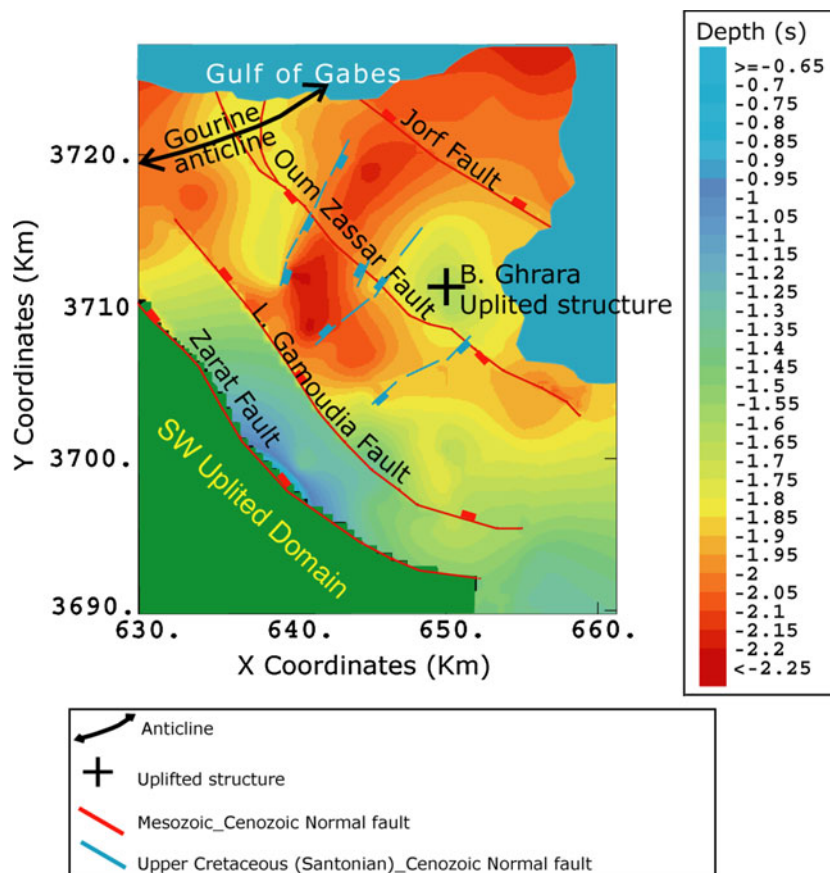


Figure 17. Structural map showing location of the master trending (NW–SE and NE–SW) faults and folds of the NE Jeffara basin.

Uplifted structure, in the eastern sector of the study area, the central downlifted domain and the Gourine anticline structure in the western sector.

The Depth Maps of the Top Aptian and Top Cenomanian

The depth maps of the Top Aptian and Top Cenomanian (Figs. 13, 14) keep, in general, the same geometric shape and the major structural elements as the Top Jurassic map. However, these structures are clearly better expressed in the Top Jurassic map than in the Top Aptian and Top Cenomanian maps.

At a regional scale, the down tilting intensity is greater for the Jurassic surface (Fig. 12) than for the Aptian (Fig. 13) and the Cenomanian (Fig. 14) ones.

This is also confirmed by the variographic analysis where the variograms (Figs. 6–8) showed that the drift increases with increasing depth of the surfaces (from Cenomanian to Jurassic). This can be explained by renewed pulses of tectonic activity mainly along the NW–SE extensional fault; hence, the resulting amount of fault displacement along the affected area may be increased for older surfaces.

At a local scale, the uplifted and downlifted structures with NW–SE directions are more pronounced than those with NE–SW directions. However, the topographic contrasts are less pronounced for the Aptian and the Cenomanian surfaces than for the Jurassic surface. This is expressed through the locally stationary structure displaying the depth variability, at a small scale, within each compartment (Figs. 6–8), as explained above in the variographic analysis. Surfaces with a more complex faulting framework are represented by variograms with relatively shorter ranges.

The Tectonic Evolution of the Study Area

A synthetic examination of the above results, based on seismo-tectonic data and variogram interpretations together with subsurface geometric modeling of the studied area was made to understand the tectonic evolution from the Mesozoic to the present. This understanding will help (i) to demonstrate the impact of tectonic evolution on the development of the major structural elements, namely the large-scale trend structures (down-tilted surfaces) and the regional scale NE–SW compartments (uplifted and downlifted zones); (ii) and finally to explain why these structural elements appear more prominent on the Top Jurassic than on the Top Aptian and Top Cenomanian maps.

Most seismic profiles in the study area remain dominated by extensional geometry. Figure 3 shows a “classic” rift-geometry basin controlled primarily by NE-dipping extensional NW–SE faults. Following the Hercynian Orogeny, a rift phase was initiated during Triassic times. During the Upper Triassic and Lower Jurassic, NE–SW extensional movements developed NW–SE normal faults leading to the setting-up of the Jeffara basin. It is elongated parallel to the faults that constitute the basin boundaries.

The study area was dominated by NW–SE normal faults and the EW faults (in the eastern domain), which were reactivated several times during the Mesozoic and Cenozoic periods. Extensional processes continued through the Jurassic and the Early Cretaceous times (Vially et al. 1994; Guiraud 1998). Faults associated with rifting continued to control sedimentation (Morgan et al. 1998). A maximum flooding event occurred during the Barremian to Aptian (Bishop 1975).

A minor, local uplift and erosion occurred and produced a tectonic unconformity, called the *Aptian unconformity* that has been identified on seismic lines (Figs. 4, 16). It is also called the “Austrian Unconformity” as it may be associated with the “Austrian tectonic phase” in the European Alps (Burlot et al. 1978). At Early and Middle Albian stages, the Jeffara domain emerged; consequently, there was no space available for sedimentation.

Extensional processes resumed in the Upper Albian time, horst and graben systems are the main structures (e.g., Boughrara structure). Associated normal faults controlled sedimentation (Morgan et al. 1998). The Albian to Cenomanian Zebbagg Formation (Fig. 2) was deposited, sealing uncon-

formably the Orbata Formation. The Turonian to Campanian sediments overlie the Zebbagg Formation. They consist of the Beida formation, the Bireno formation, and the Aleg Formation. The Aleg Formation is very thick and is characterized by the “intra-Aleg unconformity” that is well expressed on seismic cross sections (Fig. 16).

Even where it is visible, the compressional overprint is generally subtle compared to the extensional fault geometry. However, a critical examination of the geometry reveals, as illustrated on a seismic cross section perpendicular to the main structural direction (Fig. 16), the following: (i) a thickening, from SE to NW, of Lower Cretaceous (Albo-Aptian to Cenomanian) and Lower Upper Cretaceous (Turonian to Santonian) sequences across the faults indicating early extension; yet (ii) an elevation of the Top Lower and Upper Cretaceous horizons in the Hanging Wall anticline relative to Foot wall; (iii) a thinning and northwestward overlapping of the uppermost Cretaceous sequence onto the fold forelimb from the Foot Wall to Hanging Wall anticline, indicating a slight inversion; and (vi) the uppermost Cretaceous sequences become thinner and are overlapping the Mesozoic Upper Cretaceous.

Figure 16 reveals a compressional inversion that occurred locally in Santonian time; the area underwent compressional stress that deformed the sedimentary series in a ductile fashion (Guiraud 1998; Morgan et al. 1998). Several uplifted structures were developed; the most prominent one in the study area is the N80E Gourine fold (Figs. 16, 17). Following a widespread Santonian unconformity *intra-Aleg unconformity* (Figs. 4, 16), the area underwent renewed extension and subsidence as indicated by a northwest thickening of the sedimentary series from SE to NW. Finally, a gentle uplift occurred in the Late Cretaceous to Paleocene (Burlot 1967a), resulting in erosion of the Abiod and El Haria Formations and producing a tectonic unconformity (Figs. 2, 3, 16). The tertiary sedimentary sequences overlap the Mesozoic Upper Cretaceous ones and thicken northeastward (Fig. 16). During the tertiary, regional subsidence and a northeastward tilt of the area occurred in response to the Miocene northeast-southwest extension.

Consequently, the Mesozoic–Cenozoic tectonic evolution can be reconstructed through three events that strongly influenced the geometry of the Lower Cretaceous reservoirs and more generally the entire sedimentary series in the study area (Figs. 3, 16, 17)

- (i) The NW–SE trending normal faults, which involved the large-scale trend structure represented by the down-tilted surfaces, are related to the NE–SW trending regional extension accompanying the Tethyan rifting in the Jeffara basin (Bouaziz et al. 2002; Patriat et al. 2003). This extensional context was associated with continuous subsidence of variable intensity. In this context, anisotropic behavior of directional variograms would give more details on subsidence intensity variability. However, the anisotropic behavior of the drift component of the directional variograms of each surface, as shown above in the “[Variogram behavior interpretation](#)” section reproduces the directional variation of the down-tilting rate, through the drift component. Figures 6–8 show that the drift component reveals a maximum variability in the NE direction for the three, Jurassic, Aptian, and Cenomanian, surfaces. This implies that the down-tilting rate is higher in the NE direction and could announce a more intense subsidence along this direction. The reactivation of the NW–SE trending normal faults during the Albian generated the NW–SE horst and graben structures (Bougrara uplifted structure) (Figs. 3, 17).
- (ii) The minor regional-scale uplifted and downlifted structures are visible in the NE–SW direction (Figs. 16, 17) and have been derived directly from the following later events. The Santonian event resulted from onset of the collision between the African and Eurasian plates. The Jeffara basin was inverted and folded, the Gourine anticline developed on the NW side of the study area. Later, new stress-fields favored NW–SE extension with minor normal faults striking NE–SW generated the compartmentalization of the study area along the NW–SE direction. Finally, the fact that these structural elements appear more prominent in the Top Jurassic than in the Top Aptian and Cenomanian maps may be explained by the renewed pulses of tectonic activity mainly along the NW–SE extensional fault throughout geologic times. The resulting amount of fault displacements in the affected areas may be intensified in older layers and more explicitly on Cenomanian to Jurassic surfaces.

CONCLUSIONS

This article presents a case study of a faulted-reservoir where seismic information, oil well data and geostatistical tools were used. Geostatistical reservoir modeling uses the variogram as a tool to measure the spatial variability of the geologic medium under study before making any estimation or simulation. In our case study, we demonstrate that variogram modeling depends not only on data statistics and on the variogram shape, but also on additional information drawn from a geologic analysis of available data. Thus, the link between geologic knowledge and experimental variogram behavior must be understood to achieve a reliable variogram interpretation and modeling constraints needed to optimize reservoir characterization. The methodology presented here provides a framework for describing experimental variogram behavior and interpreting the variogram components at different length scales and in different directions.

From the basic geologic knowledge, we showed that the architecture of the study area is characterized by a regional-scale trend of down-tilted surfaces and local-scale lateral NW–SE and NE–SW compartments of uplifted and downlifted structures. In the interpretations of variograms, these geologic characteristics are expressed through the drift and local stationary structures. The hole effect in the variogram reflects the existence of repetitive stepped or collapsed compartments in the study area. The attenuation of the hole effect at long distances on each one of the variograms reveals that the slip displacement magnitude of the faults decreases toward the Mediterranean Sea.

Concerning the variogram modeling, the understanding of the geologic mechanisms that control the variogram shape with its different components provided useful information to select a representative variogram model for each depth variable. For each local estimation using kriging, we have to use only the immediate neighbors of any point to be predicted, situated inside the compartment of interest so as to work with a small data variance and, thus, respect the spatial continuity/variability of the phenomenon under study. Accordingly, the variograms were fitted on the basis of their behavior toward small and medium distances; only the stationary features were taken into account for depth interpolation. Despite of this assumption, the trends predicted by variography and their anisotropic behavior match those interpreted

from the estimated surface maps. In turn, the variogram behavior provided some criteria which were used as a guide for further geologic observations. A sensitivity analysis of the different variograms in different directions and a comparison of their parameters from one horizon to another were very useful to evaluate some important assumptions. This required a study of the tectonic evolution of the study area integrating the original data and the different modeled surface maps, to identify its impact on the estimated prominent structural elements. In fact, subsidence and uplift, related to movements along various NW–SE and NE–SW normal faults and local compressional events, strongly influence the occurrence of uplifted reservoir structures and the geometry of the bounding surfaces. The anisotropic behavior, mainly of the drift and the hole effect components, of the variograms, reveals that the rate of down-tilting changes with the direction and is higher in the NE direction. The slip displacement of the fault decreases toward the Mediterranean Sea.

Finally, the tectonic evolution study proved that the renewed pulses of NW–SE extensional fault movements intensified the amount of fault displacements along the affected areas throughout geologic times. This would explain the fact that the structural elements, mainly the uplifted reservoir structures, appear more prominent on the Top Jurassic than on the Top Aptian and Top Cenomanian maps.

The methodology presented here for reservoir architectural modeling requires the use of a systematic variogram interpretation and of a modeling procedure that necessarily integrates geologic knowledge. This procedure is very useful for assessing the importance of the assumptions made to deduce the variogram type and the bounds for its parameters. Such a methodology can be employed effectively in many other geostatistical analyses. One important goal of the present architectural modeling is that it would be used as essential input, with petrophysical properties such as porosity and permeability, into fluid-flow simulations. However, surface time maps would have to be converted into depth maps (in meters) through seismic time-depth conversion.

ACKNOWLEDGMENTS

The authors would like to thank Entreprise Tunisienne des Activités Pétrolières (ETAP) for

providing seismic and well data. The authors gratefully acknowledge helpful discussions with Prof. Ghislain De Marsily, Dr. Christian Ravenne, and Prof. Jean-Paul Chilès.

REFERENCES

- Bishop, W. F. (1975). Geology of Tunisia and adjacent parts of Algeria and Libya. *Association of Petroleum Geologists Bulletin*, 59(3), 413–450.
- Bodina, S., Petitpierre, L., Wooda, J., Elkanounib, I., & Redf-erna, J. (2010). Timing of early to mid-cretaceous tectonic phases along North Africa: New insights from the Jeffara escarpment (Libya–Tunisia). *Journal of African Earth Sciences*, 58(3), 489–506.
- Bouaziz, S. (1990). Geologic map of Medenine (1/100,000).
- Bouaziz, S., Barrier, E., Angelier, J., Tricart, P., & Turki, M. M. (1998). Tectonic evolution of Southern Tethyan margin in southern Tunisia. In S. Crasquin-Soleau & E. Barrier (Eds.), *Peri-Tethys Memoir: 3. Stratigraphy and Evolution of Peri-Tethyan Platforms. Bulletin du Museum National d'Histoire Naturelle*, 177, 215–236.
- Bouaziz, S., Barrier, E., Turki, M. M., Tricart, M., & Angelier, J. (2002). Tectonic evolution of the Southern Tethyan margin in Southern Tunisia. *Tectonophysics*, 357, 227–253.
- Burrollet, P. F. (1967). General geology of Tunisia. In L. Martin (Ed.), *Guidebook to the geology and history of Tunisia: Petroleum exploration society of Libya* (pp. 51–58). Tripoli, Libya: Ninth Annual Field Conference.
- Burrollet, P. F. (1991). Structures and tectonics of Tunisia. *Tectonophysics*, 195, 359–369.
- Burrollet, P. F., Mugniot, J. M., & Sweeney, P. (1978). The geology of the Pelagian block—the margins and basins of southern Tunisia and Tripolitani. In A. E. M. Nairn, W. H. Kanes, & F. G. Stehli (Eds.), *The ocean basins and margins* (Vol. 4B, pp. 331–359). New York: Plenum Press.
- Busson, G. (1967). Le Mésozoïque saharien, 1re partie: l'extrême-Sud tunisien. Publications du Centre National de Recherches Scientifiques (CNRS). Paris: Série Géologique, 8, 194 pp.
- Castany, G. (1954). L'accident Sud-tunisien, son âge et ses relations avec l'accident sud-atlasique d'Algérie. Note H. Devaux, *Bulletin de la Société Française de Physique*, 184 pp.
- Chihi, H. (2000). *Modélisation 3-D des unités stratigraphiques et simulation des faciès sismiques dans la marge du golfe du Lion*. Paris: Éditions Technip.
- Chihi, H., Galli, A., Ravenne, C., Tesson, M., & de Marsily, G. (2000). Estimating the depth of stratigraphic units from marine seismic profiles using non stationary geostatistics. *Natural Resources Research*, 9(1), 77–95.
- Chihi, H., Jannée, N., Yahyaoui H., Belayouni H., & Bedir M. (2012). Geostatistical optimization of water reservoir characterization case of the “Jeffara de Médenine” aquifer system (SE Tunisia). In *Proceedings of the 6th International Conference: Water Resources in Mediterranean Basin (WATMED6), 10–12 October 2012, Sousse (Tunisia)* (pp. 437–444).
- Chihi, H., Tesson, M., Galli, A., de Marsily, G., & Ravenne, C. (2007). Modélisation géostatistique (3D) des surfaces enveloppe d'unités stratigraphique à partir de profils sismiques: exemple de la partie médiane (Languedoc) de la plate-forme continentale du Golfe du Lion. *Bulletin de la société Géologique de France*, 1, 25–39.
- Chilès, J. P., & Delfiner, D. (2012). *Geostatistics: Modelling spatial uncertainty*. New York: Wiley.
- Edward, H. I., & Srivastava, M. R. (1989). *Applied geostatistics*. Oxford: Oxford University Press.

- Entreprise Tunisienne d'Activités Pétrolières. (1997). *Tunisian stratigraphic chart*. Tunisia: Entreprise Tunisienne d'Activités Pétrolières.
- Fossen, H. (1996). Properties of fault populations in the Gullfaks Field, northern North Sea. *Journal of Structural Geology*, 18(2/3), 179–190.
- Gauthier, B. D. M., & Lake, S. D. (1993). Probabilistic modelling of faults below the limit of seismic resolution in Pelican Field, North Sea, offshore United Kingdom. *American Association of Petroleum Geologists Bulletin*, 77, 761–777.
- Geovariances, ISATIS. (2012). Technical references. Fontainebleau, France.
- Goovaerts, P. (1997). *Geostatistics for natural resources evaluation*. Oxford: Oxford University Press.
- Gringarten, E., & Deutsch, C. V. (1999). Methodology for variogram interpretation and modeling for improved reservoir characterization. Paper SPE 56654.
- Guiraud, R. (1998). Mesozoic rifting and basin inversion along the northern African Tethyan margin: An overview. In D. S. Macgregor, R. T. J. Moody & D. D. Clark-Lowes (Eds.), *Petroleum geology of North Africa* (pp. 217–229). London: Geological Society. London: Special Publication 132.
- Journel, A. (1977). *Géostatistique Minière*. Doctoral es-Sciences Thesis. Ecole des Mines de Paris, Fontainebleau.
- Klett, T. R. (2001). Total petroleum systems of the Pelagian Province, Tunisia, Libya, Italy, and Malta, the Bou Dabbous–Tertiary and Jurassic–Cretaceous Composite. *U. S. Geological Survey Bulletin*, 2202-D, version 1.0, 149 pp.
- Letouzey, J., & Trémolières, P. (1980). Paleostress fields around the Mediterranean since the Mesozoic derived from microtectonics: Comparisons with plate tectonic data. In *Géologie des chaînes alpines issues de la Téthys. 26ème C.G.I., Paris* (pp. 261–273). Mémoire du Bureau de recherches géologiques et minières, 115.
- Matheron, G. (1982). *Pour une analyse Krigeante des données régionalisées*. Technical Report N-732. Ecole des Mines de Paris Library (Fontainebleau). France.
- Morgan, M. A., Grocott, J., & Moody, R. T. J. (1998). The structural evolution of the Zaghouan-Ressas Structural Belt, northern Tunisia. In D. S. Macgregor, R. T. J. Moody, & D. D. Clark-Lowes (Eds.), *Petroleum geology of North Africa*. London: Geological Society (pp. 405–422). London: Special Publication 132.
- Mzoughi, M., Dufaure, P., & Peybernès, B. (1992). Données nouvelles sur le Jurassique du Golfe de Gabès autour de l'île de Djerba (Tunisie). *Comptes Rendus de l'Académie des Sciences* (pp. 565–570), Paris 315 II.
- Olea, R. A. (1994). Fundamentals of semi-variogram estimation, modeling, and usage. In J. Yarus & R. L. Chambers (Eds.), *Stochastic modeling and geostatistics principles, methods and case studies* (pp. 27–35). Tulsa, OK: American Association of Petroleum Geologists Bulletin.
- Patriat, M., Ellouz, N., Deyb, Z., Gaulier, J. M., & Ben Kilani, H. (2003). The Hammamet, Gabès and Chotts basins (Tunisia): A review of the subsidence history. *Sedimentary Geology*, 56, 241–262.
- Rouatbi, R. (1967). *Contribution à l'étude hydrogéologique du Karst en Terre de Gabès Sud*. PhD thesis, Montpellier.
- Sahin, A., Ghorri, S. G., Ali, A. Z., El-Sahn, H. F., Hassan, H. M., & Al-Sanounah, A. (1998). Geological controls of variograms in a complex carbonate reservoir, Eastern Province, Saudi Arabia. *Mathematical Geology*, 30(3), 309–322.
- Salaj, J. (1978). The geology of the Pelagian block: The eastern Tunisian platform. In A. E. M. Nairn, W. H. Kanes, & F. G. Stehli (Eds.), *The ocean basins and margins* (Vol. 4B, pp. 361–416). New York: Plenum Press.
- Samal, A. R., Sengupta, R. R., & Fifarek, R. H. (2011). Modelling spatial anisotropy of gold concentration data using GIS-based interpolated maps and variogram analysis: Implications for structural control of mineralization. *Journal of Earth System Science*, 120(4), 583–593.
- Scott, R. W., Azpirixaga, I. & Taylor, C. K. (1997). Carbonate platform seismic sequence attributes, Maracaibo Basin, Venezuela. In K. J. Ibrahim Palaz & K. J. Marfurt (Eds.), *Carbonate seismology*, Vol. 6 (pp. 425–443). Oklahoma: Geophysical Development Series.
- Vially, R., Letouzey, J., Bénard, F., Haddadi, N., Desforges, G., Askri, H., et al. (1994). Basin inversion along the North African margin—the Saharan Atlas (Algeria). In F. Roure (Ed.), *Peri-Tethyan platforms* (pp. 79–117). Paris: Éditions Technip.
- Yarus, J. M., & Kramer, K. (2006). Practical geostatistics—an arm-chair overview for petroleum reservoir engineers. *Journal of Petroleum Technology*, 78–87. http://www.geovariances.com/IMG/pdf/ArticleJPT_Nov2006-Yarus-Chambers.pdf.